Spatially Complete Global Spectral Surface Albedos: Value-Added Datasets Derived from Terra MODIS Land Products

Eric G. Moody, Michael D. King, *Senior Member, IEEE*, Steven Platnick, Crystal B. Schaaf, *Member, IEEE*, and Feng Gao, *Member, IEEE*

IEEE Transactions on Geoscience and Remote Sensing

Manuscript submitted April 21, 2004.

E. G. Moody is with L-3 Communications Government Services, Inc., Vienna, VA 22180 USA (e-mail: moody@climate.gsfc.nasa.gov).

M. D. King and S. Platnick are with the Earth Sciences Directorate, NASA Goddard Space Flight Center, Greenbelt, MD 20771 USA.

C. B. Schaaf and F. Gao are with Center for Remote Sensing, Department of Geography, Boston University, Boston, MA 02215 USA.

Abstract–Recent production of land surface anisotropy, diffuse bihemispherical (white-sky) albedo and direct beam directional hemispherical (black-sky) albedo from observations acquired by the MODIS instruments aboard NASA's *Terra* and *Aqua* satellite platforms have provided researchers with unprecedented spatial, spectral, and temporal information on the land surface's radiative characteristics. Cloud cover, which curtails retrievals, and the presence of ephemeral and seasonal snow limit the snow-free data to approximately half the global land surfaces on an annual equal-angle basis. This precludes the MOD43B3 albedo products from being used in some remote sensing and ground-based applications, climate models, and global change research projects.

An ecosystem-dependant temporal interpolation technique is described that has been developed to fill missing or seasonally snow-covered data in the official MOD43B3 albedo product. The method imposes pixel-level and local regional ecosystem-dependent phenological behavior onto retrieved pixel temporal data in such a way as to maintain pixel-level spatial and spectral detail and integrity. The phenological curves are derived from statistics based on the MODIS MOD12Q1 IGBP land cover classification product geolocated with the MOD43B3 data. The resulting snow-free value-added products provide the scientific community with spatially and temporally complete global white- and black-sky surface albedo maps and statistics. These products are stored on one-minute and coarser resolution equal-angle grids, and are computed for the first seven MODIS wavelengths, ranging from 0.47 through 2.1 μm, and for three broadband wavelengths, 0.3-0.7, 0.3-5.0 and 0.7-5.0 μm.

I. INTRODUCTION

Land surface albedo is an important parameter in describing the radiative properties of the earth's surface. It represents the ratio of reflected radiation to incoming solar radiation at the earth's surface, and is important for the remote sensing of atmospheric aerosol [16], [21], [24], and cloud [23], [25], [34] properties from space, ground-based analysis of aerosol optical properties from surface-based sun/sky radiometers [12], [15], biophysically-based land surface modeling of the exchange of energy, water, momentum, and carbon for various land use categories [5], [42], and surface energy balance studies [11], [17], [49]. These projects require proper representation of the surface albedo's spatial and spectral variation, due in part to the distribution of vegetated surface types and growing conditions, and temporal variations, due largely to changes in the amount of vegetation over phenological growth cycles [1]-[4], [6], [7], [9], [10], [14], [24]-[26], [29], [30], [37], [41]-[46], [50]. These representations are often lacking in datasets prior to the latest generation of land surface albedo products [8], [27], [33].

The launch of the Moderate Resolution Imaging Spectroradiometer (MODIS) onboard NASA's *Terra* [22] and *Aqua* [31] spacecraft in December 1999 and May 2002, respectively, ushered in a wealth of new products with unprecedented spectral, spatial, and temporal characteristics. Of particular interest to the present study is the operational diffuse bihemispherical (white-sky) and direct beam directional hemispherical (black-sky) land surface albedo dataset, known as MOD43B3 [38]. This product is a validated [18], [19], [28], [47] 16-day aggregate global dataset at 1 km spatial resolution for the first seven MODIS bands, 0.47 through 2.1 μm, and for three broadband wavelengths, 0.3-0.7, 0.3-5.0, and 0.7-5.0 μm. These albedo measurements are intrinsic properties of the surface and can be combined as a function of diffuse-sky light to obtain actual albedo values

(blue-sky) that are equivalent to those measured by albedometers at the ground. These dataset characteristics afford the necessary spatial, spectral, and temporal resolutions to accurately provide radiative properties of the surface for inclusion in a variety of earth system research projects. However, roughly half the global land surface on an annual equal-angle basis is obscured due to persistent and transient cloud coverage as well as ephemeral and seasonal snow effects. The direct inclusion of the MOD43B3 product into either land surface models or remote sensing applications is thereby hindered or precluded because of these extensive spatial data gaps and the desire of modelers to work with snow-free albedos.

The goal of the present study is to provide researchers with the requisite spatially complete global snow-free land surface albedo datasets by filling in missing data from the official MOD43B3 dataset with geophysically realistic values supplied by an ecosystem-dependent temporal interpolation technique. The technique is based upon the concept that within a limited region, pixels of the same ecosystem classification should exhibit roughly the same phenological, or temporal, behavior; that is the pixels should begin to green-up, reach full growth, begin to senesce, and reach full dormancy at approximately the same time and with the same amplitude [20], [32], [36], [39], [40], [48], [51]. However, this similarity in the shape of the ecosystem's behavioral curve does not preclude pixel-to-pixel differences in the relative magnitudes of the behavioral curves due in part to spatial variations in growing conditions from climate and soil differences. In order to maintain these spatial pixel-level variations in a temporal sense, missing data are filled in by imposing the shape of the pixel's ecosystem classification phenological curve onto the temporal data that does exist for that pixel.

Generating these value-added products requires multiple steps, including (i)

remapping the native MOD43B3 data stored in Sinusoidal (SIN) projection onto one-minute climate modeling (equal-angle) grids (CMG), (ii) applying the appropriate quality assurance (QA) information to remove retrievals over water and lesser quality and ephemeral snow data, (iii) filling missing data with the ecosystem-dependent temporal interpolation technique (using the MODIS MOD12Q1 International Geosphere-Biosphere Programme (IGBP) ecosystem classification dataset [13]), and (iv) storing both the original and filled data as well as the original and fill-technique QA into new Hierarchical Data Format (HDF) files. For research projects that require coarser resolution, statistical maps of the filled product are also generated at reduced resolutions.

II. Ecosystem-Dependent Temporal Interpolation Technique

The primary design criterion for developing a technique for filling missing data was to maintain the detail and integrity of pixel-level information by using geophysically realistic statistics based on data that was available local to that pixel. When data from one wavelength are missing due to cloud or unacceptable due to snow effects, then data from the other wavelengths are also unlikely to be available. Techniques based purely on spatial averaging were also not considered, as there are large regions (such as the tropics) that have such poor spatial coverage that data that are simply too far from the pixel end up influencing the replacement values. The only viable option is to use temporal information.

There is a chance that a pixel has adequate temporal coverage to be able to perform simple splines to fill missing temporal data in a meaningful way. However, with this particular dataset a majority of pixels do not have sufficient yearly temporal coverage to properly represent the entire snow-free growth cycle or cycles. Fortunately, it was more likely that statistics gathered from pixels of the

same ecosystem class within a limited region surrounding the pixel would have the requisite temporal coverage. Thereby, the MODIS IGBP ecosystem classification was used as the inherent link to relate the regional phenological information to the pixel-level information [13].

Within a small region, pixels of the same ecosystem class should exhibit similar growth or phenological behavioral curves [20], [32], [36], [39], [40], [48], [51], which describe how the vegetation of an ecosystem changes temporally. Each ecosystem class should enter successive phenological stages (green-up, full maturity, senescence, and dormancy) at approximately the same time and with the same amplitude. Therefore the shape of the ecosystem's pixel-level and regional behavioral curves should be very similar. Pixel-to-pixel variations in growth conditions, however, result in variations in magnitude of the behavioral curves, as shown in Fig. 1a.

Exploiting this inherent link, an ecosystem classification-dependent temporal interpolation technique was developed that utilizes pixel-level and regional ecosystem-dependent phenological behavioral curves and the high quality temporal data that are available for that pixel. First, the shapes of the pixel's and region's ecosystem phenological curves are determined using the extant temporal data points from both the pixel and from statistics computed for a region using pixels with the same ecosystem classification. Then to ensure that both the temporal behavior of an ecosystem class and the pixel-to-pixel variations in magnitude are maintained, the shape and only the shape of the curves are imposed onto the pixel's valid temporal data by computing an average offset between pixel data and the behavioral curves, as shown in Fig 1b. The pixel's missing temporal data can then be filled in from the pixel's curve or from one of the regional curves, depending on what curve is deemed to provide the best information.

This general technique, described in detail in Section III, has to be modified in regions where valid retrievals are scarce or unacceptable, such as in (i) tropical regions that are affected by persistent cloud systems from the Intertropical Convergence Zone (ITCZ), (ii) missing observations for extended seasons, such as the monsoon seasons in India and Southeast Asia, or (iii) regions where the dormant state is not observed due to a combination of cloud and seasonal snow onset, mostly at high latitudes.

III. Methodology for Generating Spatially-Complete Albedo Products

The temporal interpolation technique described in section II is employed to generate snow-free spatially complete albedo products, both white-sky and black-sky, at the first seven MODIS wavelengths and for three broadband wavelengths. This is accomplished by analyzing one year of global MOD43B3 data from *Terra* in order to take advantage of at least one full growth cycle and phenological curve. Before this technique can be applied, however, the MOD43B3 data must be conditioned and the statistics by IGBP ecosystem class generated. Once the data are ready to be filled in, global processing occurs for each land pixel by determining the best processing path based on the available temporal coverage. Each pixel can be filled in by either a general method or through specialized algorithms that handle seasonally or permanently snow-affected regions and areas of persistent cloud cover. The following sections detail the data conditioning, the statistical workup, the phenological curve calculations, and the methodologies employed to apply the temporal interpolation technique.

A. MODIS Albedo and Ecosystem Dataset Conditioning

The MOD43B3 16-day global albedo product is stored in a Sinusoidal (SIN) projection with a series of approximately 400 tiles (one 10° x 10° tile per file). To

better conform with MODIS atmosphere global products and processing, and to ease integration into modeling efforts, as well as facilitate analysis in the current project, the raw data and QA are mosaiced onto a one-minute spatial resolution equal-angle climate modeling grid (CMG), which is ~2 km in spatial resolution at the equator. This procedure is a sampling process for which the CMG grid is defined and the data and QA from the nearest geolocated pixel in the MOD43B3 tile are copied to the CMG grid.

The data are also conditioned by applying the MOD43B3 general and band-specific QA to remove pixels of lower quality. As detailed in the user guide and [38], pixels with less then 3 observations over the 16-day period were replaced with a fill-value as there were not enough observations to have confidence in the retrieved albedo value. Pixels flagged as seasonally snow-covered or over ephemeral waters were also replaced with fill-values, as the current study intends to provide seasonal snow-free land albedo products. In addition, a polar darkness model, based on data and software freely available from the US Naval Observatory's Astronomical Applications Department (aa.usno.navy.mil), defined regions for which no replacement values would be supplied due to low solar illumination.

Fig. 2 shows the resulting 0.86 μm MODIS white-sky albedo for four seasons, remapped and with quality assurance applied as described above. Roughly half the global land surface, on a yearly equal-angle basis, is obscured due to persistent and transient cloud cover as well as ephemeral or seasonal snow effects that do not allow for sufficient observations of the underlying surface. At a minimum, roughly a quarter of the land surface is obscured during July and August, most notably due to cloud cover from the ITCZ, whereas a maximum of about 60-65% of the land surface is either obscured by cloud or covered by seasonal

snow during January and February.

In a similar manner, the MOD12Q1 static ecosystem classification product is reprojected onto a one-minute spatial resolution equal-angle CMG grid, but only for the IGBP classification scheme and associated QA arrays. This remapped dataset is instrumental in generating statistics by ecosystem class and for implementing the temporal interpolation technique. At present, no QA is applied to the reprojected IGBP map, and only the predominant ecosystem classification is used for each pixel.

B. Required Statistics

As described in Section II, regional ecosystem-dependent phenological curves play a critical role in the temporal interpolation technique, and the size of the regions needed to provide adequate temporal coverage varies globally due to the amount of cloud and seasonal snow cover, as can be seen in Fig. 2. In order to provide temporally adequate phenological curves for all scenarios, a range of regional sizes surrounding a pixel were considered, beginning with a 0.5° x 0.5° latitude–longitude regional size and ranging up to 10° x 10°, 10° x 20°, and 10° x 30° regional sizes. The latitudinal region size was curtailed to 10° to reflect the dominant latitudinal seasonal dependence in phenological growth cycles while the longitudinal size was less restrictive following the climate stratification. Smaller box sizes should more closely reflect pixel-level trends, and the methodology for selecting the phenological curve is heavily biased towards using smaller box sizes.

Ideally, one would compute the simple statistics of the mean, standard deviation, and number of points, for each regional size centered around each pixel on the global map, however data volume make such calculations intractable for

global processing. Instead, CMG grids are defined based on the various regional sizes, and the statistics, by IGBP ecosystem class, are computed from the conditioned pixel-level data inside each region. In order to ensure only the highest quality data are used for the statistical generation, an additional QA constraint was imposed such that only pixel-level data with at least seven observations per 16-day period are included in the statistical calculations.

C. Temporal Curve Calculation

Over the course of a year an ecosystem can exhibit one or more complete phenological growth cycles. For example, ecosystems at high latitudes typically exhibit one growth cycle per year due to the limited amount of solar radiation. Drought dependant ecosystems in the tropics however often exhibit two complete cycles resulting from the availability of moisture as the ITCZ migrates northward and southward of the equator. As a result, in order to capture at least one complete phenological growth cycle, the temporal interpolation technique must be applied to a full year of data. It was found however that in regions that have sufficient temporal coverage better representation can be achieved by using data over half-year sections.

For the general methodology, ecosystem phenological behavior is represented over two half-year sections that span northern hemisphere winter to summer (including the 16-day periods from days 1 through 177) or that span northern hemisphere summer to winter (including the 16-day periods from days 193 through 353). The breaks in the half-year sections often occur during the periods of phenological full growth or full decay for temperature dependent vegetation when albedo values should be changing at the slowest rates. To ensure that an ecosystem's phenological behavior for both sections are continuous at

day 193, the temporal behavioral curves are computed with the additional two 16-day periods that overlap day 193. While this is not as strict as a derivative check, the extra days generally include some of the beginning senescence or end of the green-up periods, such that continuity is well represented.

Although several methods could be employed to prescribe an ecosystem's phenological behavior of the valid data over the half-year section, such as Logistic functions [51], in the interest of computational time, a weighted least-squares polynomial fit [35] was employed. To better describe the available data and reduce the inherent vacillations of polynomial fits while maintaining the ability to describe multiple growth cycles, the order of the polynomial varied from first to third order. The order was selected based upon the overall temporal coverage, and if the end points of the half-year sections had valid data. In addition, for half-year sections for which the end points were missing, attempts were made to reduce the oscillations in the tails of the polynomial fits by fixing the end points of the section to the nearest neighboring temporal point. Fits using regional statistical data were also weighted by the standard deviation in order to place an emphasis on temporal data with less variability or more observations.

D. General Methodology

The majority of land pixels reside in areas where either the pixel itself or some small region surrounding the pixel has adequate temporal coverage from which the phenological curve of the pixel's ecosystem can be prescribed. The deciding factors on whether to use the pure pixel or the regional information for the same ecosystem lie in how much of the temporal curve contains valid data and if the existing data adequately describe the phenological stages.

It was determined that if 70% of a pixel's half-year sectional data are valid

and are sufficiently spread throughout the half-year section, a phenological curve can be computed from pixel-level data and therefore missing values can be computed directly from the pixel's phenological curve. If this criterion is not met, then phenological curves for the pixel's ecosystem class are computed for all statistical region sizes and offsets applied to impose the shape of the curves onto the pixel's valid data. The statistical curves are evaluated to determine which curve has the best combination of temporal coverage along with which one best represents the pixel-level data, based on deviation from pixel-level data. A bias is imposed towards selecting smaller regional sizes, which should be more representative of pixel-level behavior, and then the selected statistical curve is used to fill in the missing data. In addition, a check ensures that the statistical curves have decidedly better temporal coverage and phenological representation; otherwise pixel-level information is used to perform the filling. This general methodology was able to represent single or multimodal phenological cycles.

For example, much of the continental United States is processed with this general methodology, as there is adequate pixel or local regional temporal coverage for the ecosystem phenological curves to be discerned. Fig. 3 demonstrates the general temporal interpolation technique applied to a pixel of Midwest cropland. The pixel's temporal coverage is only about 40%, but the local region's ecosystem statistics can cover up to 90%. Once the offset is applied and the statistical curves compared, the decision methodology chose the 1° x 1° regional statistical curve to fill in the missing pixel-level data points. This general methodology was also applied to the deciduous broadleaf forests of the northeastern US (shown in Fig. 1). However, in this case there was ~80% pixel temporal coverage with adequate spacing, so the missing data were filled using the pixel-level phenological curve. Fig. 4 compares the conditioned MOD43B3 and spatially com-

plete 0.858 μm data for the end of May in the continental United States, an area where most of the pixels were processed using the general methodology. Notice that the unique pixel-level information is well maintained and the local and regional growth cycles are at different stages of development (especially for cropland in Iowa as compared to other Midwestern states and along the Mississippi River basin).

1) Methodology for Seasonal Snow Cases: At high latitudes, the end of the senescence stage and the full dormancy stage are often obscured by cloud and covered by snow for large regions, resulting in incomplete phenological curves for both the pixel and even the largest of the regional statistics. As one goal of the current study is to provide seasonal snow-free albedo maps, the full decay state must be approximated in order to properly represent the full phenological curve. As there is typically only one growth cycle and the full maturation state is usually observed in high latitudes, the full decay state can be approximated as an ecosystem-dependent percentage of the full maturation albedo value.

These ecosystem-dependent percentages can be obtained from observations at moderately high latitudes that are affected by seasonal snow cover, but whose full decay state is observed. These percentages are computed for each ecosystem class and wavelength over the Northern Hemisphere and separated into Eastern and Western regions. The percentages can then be applied to each pixel-level and regional statistical curves in both the Southern and Northern Hemispheres to approximate the full decay state. Table I contains sample percentages of the decrease in white-sky albedo between the full growth and full decay phenologies for a selection of ecosystem classifications and wavelengths. These percentages are computed from valid MOD43B3 data that have proper representation of both seasons, and are separately computed for the western and eastern hemispheres.

Implementation of the percentages for these seasonally snow-affected regions involves a slight modification to the general methodology. At latitudes higher than 40° or if any pixel's temporal point has been flagged as having seasonal snow, the algorithm will determine if pixel and regional statistical phenological curves have adequately described the full decay state. If so, then they are processed with the general methodology; however if the full decay is not seen in the pixel or regional data, then the winter end point is computed to be the ecosystem-dependent percentage of the maximum albedo during the full maturation stage. In addition, the rules for selecting the pixel or statistical curve for filling are modified to reflect the lack of full seasonal data. If a pixel has over 40% coverage and an observed summertime maximum, pixel-level phenological curves are used as they have adequate or comparable coverage to the statistical curves. Otherwise, statistical curves are examined, ruling out curves with no full maturation coverage, and selecting the curve with the best combination of temporal coverage and fit of the pixel-level data, biasing towards smaller regional sizes.

Fig. 5 shows an example for the Siberian mixed forest ecosystem classification in which neither the pixel nor regional statistics observe the full white-sky albedo decay, but instead have the full decay approximated. In this case, the pixel-level curve was selected as it had similar temporal coverage as the regional statistics. Fig. 6 compares the conditioned MOD43B3 and filled white-sky albedo at 0.858 μm for the end of November for Europe and western Asia. Notice that even though this region is in full decay with very little snow-free and cloud-free observations, the pixel-level detail is maintained due to use of pixel-level magnitude together with ecosystem-dependent full decay percentages.

2) Methodology for Permanent Snow and Ice Cases: Permanent snow and ice

cases deviate significantly from the general methodology because of poor temporal coverage of the melt season, especially in high latitudes. Instead of computing and applying phenological curves on a half-year basis, the entire year of data is utilized in one of two ways. If the pixel has at least one valid temporal data point during the year, a mean is computed for each wavelength from the pixel's valid temporal data and the corresponding means are substituted for each of the missing days. If the pixel does not have any valid days for the year, wavelength dependent statistical means are substituted for every day. The statistics are generated from central Greenland, which has the largest tract of contiguous permanent snow ecosystem classification. Admittedly, this method does not capture the temporal nature of the permanent snow ecosystem class and will be an area for future consideration.

3) Methodology for Persistent Cloud Cases: Equatorial regions with large amounts of water vapor and regions affected by monsoon seasons, such as India and Southeast Asia, experience periods of cloud cover that preclude observations for single or multiple seasons or sometimes nearly the entire year. For these situations, the phenological behavior is either incomplete or consists of statistically small samples, even over the largest regional sizes considered in the general methodology. Computing statistics over latitudinal belts that cover continental or sub-continental regions can, however, provide adequate phenological behavior with a sufficient sample size. For these areas, data tends to be scarce during green-up and peak growth stages due to cloud cover and rainfall, necessitating the generation of phenological curves from an entire year of data instead of half-year periods. These alterations to the general methodology provide statistics that can describe single or multimodal phenological cycles.

There are five distinct regions, summarized in Table II, that require a modi-

fied processing methodology, including parts of South America, Central Africa, the Indian subcontinent, Southeast Asia, and Oceania plus northern Australia. Over these regions, a single phenological behavioral curve is obtained for each ecosystem type, derived from statistics computed over a latitudinal belt covering a fixed longitudinal area and a fixed number of degrees of latitudes north and south of the latitude of the pixel being processed, as shown in Table II. The shape of the latitude belt's ecosystem-dependent phenological curve is then imposed on the pixel's valid temporal data in order to fill the pixel's missing temporal data.

Figs. 7 and 8 demonstrate this technique used to fill missing data on the Indian subcontinent and Africa, respectively. Although the majority of the Indian subcontinent is obscured by monsoon clouds, the pixel-level detail of the green-up stage in May appears throughout the subcontinent, including the more pronounced green-up in the Ganges Valley below the Himalayan plateau where the concentration of water vapor is the greatest. In Africa, the ITCZ has migrated towards southern Africa, leaving central Africa in the senescence stage. Also notice that there is a missing tile in Namibia during this time period, whose values were replaced by the general processing.

4) Pixels with No Temporal Coverage: There are some cases in which a pixel does not have any temporal albedo coverage whatsoever, however the ecosystem class is always known, as the MOD12Q1 Land Cover product fills from historical information if there are no MODIS observations in a specific year. To approximate pixel-level information, statistics of the same ecosystem class from the smallest possible region surrounding the pixel are substituted as pixel-level information before applying the temporal interpolation technique. A selected region must have at least three valid days in order to assure that the selected re-

gion has a significant number of observations. If no regions up to 10° x 30° have at least three valid days, the requirement is successively reduced to one day. Regions that are processed with this methodology for persistent cloud cases use data from the entire year instead of the half-year periods.

IV. PRODUCT SUMMARY

Applying the temporal interpolation technique to each pixel of the white-sky and black-sky albedo datasets and for each of the seven specific and three broadband wavelengths, results in a spatially complete snow-free global land surface albedo dataset with fine spatial, spectral, and temporal characteristics. Comparing Fig. 9 to Fig. 2, one can clearly see the results of the fill methodology on a global basis for four seasons of white-sky albedo at 0.86 μm.

The fill methodology maintains not only the temporal integrity of the dataset, but also the spectral integrity. Fig. 10 shows the white-sky albedo as a function of wavelength for a region encompassing London, England and Paris, France and for selected ecosystem classifications within the region. Note that although this figure is derived from the spatially complete dataset, it is indistinguishable from the MOD43B3 dataset for the large number of pixels of each ecosystem within this region (not shown). This figure also demonstrates the unique nature of each ecosystem's spectral signature at a fixed time, in this case June 26-July 11, 2001. These spectral signatures vary as a function of time and the distribution shown in this figure may not be so pronounced at other times of the year. For example in a single spatial region, a highly vegetated surface (cropland) and a lesser vegetated surface (urban) exhibit unique temporal signatures as well, as can be seen in Figs 11 and 11b. The full growth season of the cropland, represented by the period beginning on day 177 (June 26-July 11), exhibits much larger

white-sky albedos in the vegetative bands (around 0.86 μm) than urban ecosystems (which reflect much less solar radiation than croplands that have large canopies).

To reduce the data volume of the one-minute resolution spatially-complete albedo products in an attempt to enhance access and use of these products, the data have been stored in HDF files formatted in such a way that a user need only download and store the information that they require. Each 16-day period's data are stored in twenty separate HDF files, one per wavelength and one per white- or black-sky albedo. The QA data for each 16-day period are also stored in separate HDF files, one file for general MOD43B3 QA, seven band-specific MOD43B3 QA files, and ten band-specific value-added processing QA files. Table III highlights the file sizes of the spatially complete albedo maps.

For users that require coarser resolution, the one-minute resolution (land-only) products have been aggregated onto climate modeling grids of varying sizes, from 0.5° x 0.5°, up to 10° x 10°. Simple statistics, consisting of the mean, standard deviation, and number of data points, have been computed for each ecosystem class or as a whole, over each grid cell; however QA information is not stored. Each resolution's statistics are stored in HDF files formatted to store each 16-day period's data in four separate HDF files, one per white-sky or black-sky albedo for both statistics by ecosystem class or as a whole. Table IV highlights file sizes of these statistical reduced-size products.

Information pertaining to the production, maintenance, image gallery, data availability, and download of these value-added products are available as part of the MODIS Atmosphere Science Team website, modis-atmos.gsfc.nasa.gov, with the data and images available for public download via an anonymous ftp site, ftp://modis-atmos.gsfc.nasa.gov. Current production of spatially complete al-

bedo maps and statistics consists of 2001 and 2002 datasets.

V. CONCLUSIONS

Snow-free land surface albedo is an important parameter in various radiative transfer research and modeling initiatives. Recent observations of white-sky and black-sky land surface albedo from MODIS instruments aboard NASA's *Terra* and *Aqua* satellite platforms have provided researchers with unprecedented spatial, spectral, and temporal characteristics. Cloud cover curtails retrievals and the presence of ephemeral seasonal snow limits the snow-free albedo data to approximately half the global land surface on an annual equal-angle basis. This precludes the routine use of MOD43B3 albedo products in many earth science regional and global scale research and modeling projects.

In this paper we describe a temporal interpolation technique that has been developed to fill missing data in the official MOD43B3 albedo product. The technique imposes pixel-level and local regional ecosystem-dependent phenological behavior onto retrieved pixel data in a way that maintains pixel-level spatial and spectral detail and integrity. The resulting value-added products provide researchers with spatially-complete global white-sky and black-sky surface albedo maps and statistics, stored on one-minute and coarser resolution climate modeling equal-angle grids, for the first seven MODIS wavelengths, ranging from 0.47 through 2.1 μm, and for three broadband wavelengths, 0.3-0.7, 0.3-5.0, and 0.7-5.0 μm. The value-added products maintain the original MOD43B3 retrievals and quality assurance information, as well as provide the statistically filled values and processing quality assurance information. This product is invaluable for validating climate model outputs and projections and would be equally needed for offline driven bio-physically based land surface models that

require albedo as a lateral and initial boundary condition. It is also expected to foster earth science research with global focus.

ACKNOWLEDGMENTS

The research reported in this article was supported by the MODIS Science Team under NASA contract 621-30-04 to Goddard Space Flight Center (EGM, MDK, SP) and NASA contract NAS5-31369 to Boston University (CBS, FG). The authors would like to express their appreciation to Mr. John Hodges, Boston University, for assistance with the MOD12Q1 ecosystem classification product and Dr. Lahouari Bounoua, University of Maryland, for providing valuable insight into modeling community requirements and reviewing the methodologies used in this work.

REFERENCES

[1] G. B. Bonan, "Effects of land use on the climate of the United States," *Climatic Change*, vol. 37, pp. 449-486, 1997.

[2] G. B. Bonan, "Frost followed the plow: Impacts of deforestation on the climate of the United States," *Ecol. Appl.*, vol. 9 (4), pp. 1305-1315, 1999.

[3] G. B. Bonan, K. W. Oleson, M. Vertenstein, S. Levis, X. Zeng, Y. Dai, R. E. Dickinson, and Z.-L. Yang, "The land surface climatology of the community land model coupled to the NCAR community climate model," *J. Climate*, vol. 15, pp. 3123-3149, 2002.

[4] L. Bounoua, G. J. Collatz, S. O. Los, P. J. Sellers, D. A. Dazlich, C. J. Tucker and D. Randall, "Effects of land cover conversion on surface climate," *J. Climate*, vol. 13, pp. 2277-2292, 2000.

[5] L. Bounoua, R. DeFries, G. J. Collatz, P. Sellers, and H. Khan, "Effects of land cover conversion on surface climate," *Climatic Change*, vol. 52, pp. 29-64, 2002.

[6] J. G. Charney, "Dynamics of deserts and drought in the Sahara," *Quart. J. Royal Meteo. Soc.*, vol. 101, pp. 193-202, 1975.

[7] J. G. Charney, W. J. Quirk, S. Chow, and J. Kornfield, "A comparative study of the effects of albedo change on drought in semi-arid regions," *J. Atmos. Sci.*, vol. 34, pp. 1366-1385, 1977.

[8] I. Csiszar and G. Gutman, "Mapping global land surface albedo from NOAA AVHRR", *J. Geophs. Res.*, vol 104 (D6), pp. 6215-6228, 1999.

[9] R. E. Dickinson, "Land Surface," in *Climate System Modeling*, edited by K. E. Trenberth, Cambridge University Press, pp. 149-171, 1992.

[10] R. E. Dickinson, "Land processes in climate models," *Remote Sens. Environ.*, vol. 51, pp. 27-38, 1995.

[11] P. A. Dirmeyer and J. Shukla, "Albedo as a modulator of climate response to tropical deforestation," *J. Geophys. Res.*, vol. 99, pp. 20863-20878, 1994.

[12] O. Dubovik, A. Smirnov, B. N. Holben, M. D. King, Y. J. Kaufman, T. F. Eck, and I. Slutsker "Accuracy assessments of aerosol optical properties retrieved from AERONET sun and sky-radiance measurements," *J. Geophys. Res*., vol. 105, pp. 9791-9806, 2000.

[13] M. A. Friedl, D. K. McIver, J. C. F. Hodges, X. Y. Zhang, D. Muchoney, A. H. Strahler, C. E. Woodcock, S. Gopal, A. Schneider, A. Cooper, A. Baccini, F. Gao, and C. Schaaf, "Global land cover mapping from MODIS: Algorithms and early results," *Remote Sens. Environ*., vol. 83, pp. 287-302, 2002.

[14] A. Henderson-Sellers and M. F. Wilson, "Surface albedo data for climatic modeling," *Rev. Geophys. Space Phys.*, vol. 21, pp. 1743-1778, 1983.

[15] B. N. Holben, T. F. Eck, I. Slutsker, D. Tanré, J. P. Buis, A. Setzer, E. Vermote, J. A. Reagan, Y. J. Kaufman, T. Nakajima, F. Lavenu, I. Jankowiak, and A. Smirnov, "AERONET—A federated instrument network and data archive for aerosol characterization," *Remote Sens. Environ.*, vol. 66, pp. 1-16, 1998.

[16] N. C. Hsu, S. C. Tsay, M. D. King, and J. R. Herman, "Aerosol retrievals over bright-reflecting source regions," *IEEE Trans. Geosci. Remote Sens.*, vol. 42, pp. 557-569, 2004.

[17] W. J. Ingram, C. A. Wilson, and J. F. B. Mitchell, "Modeling climate change: An assessment of sea ice and surface albedo feedbacks," *J. Geophys. Res.*, vol. 94, pp. 8609-8622, 1989.

[18] Y. Jin, C. B. Schaaf, F. Gao, X. Li, A. H. Strahler, W. Lucht, and S. Liang, "Consistency of MODIS surface bidirectional reflectance distribution function and albedo retrievals: 1. Algorithm performance", *J. Geophys. Res.*, vol.

108 (D5), doi:10.1029/2002JD002803, 2003a.

[19] Y. Jin, C. B. Schaaf, C. E. Woodcock, F. Gao, X. Li, A. H. Strahler, W. Lucht, and S. Liang, "Consistency of MODIS surface bidirectional reflectance distribution function and albedo retrievals: 2. Validation", *J. Geophys. Res.*, vol. 108 (D5), doi:10.1029/2002JD002804, 2003b.

[20] J. Kaduk and M. Heimann, "A prognostic phenology scheme for global terrestrial carbon cycle models," *Climate Research*, vol. 6, pp. 1-19, 1996.

[21] Y. J. Kaufman, D. Tanré, L. A. Remer, E. F. Vermote, A. Chu, and B. N. Holben, "Operational remote sensing of tropospheric aerosol over land from EOS moderate resolution imaging spectroradiometer," *J. Geophys. Res.*, vol. 102, pp. 17051-17067, 1997.

[22] M. D. King, and D. D. Herring, "Monitoring Earth's vital signs," *Sci. Amer.*, vol. 282, pp. 72-77, 2000.

[23] M. D. King, Y. J. Kaufman, W. P. Menzel, and D. Tanré, "Remote sensing of cloud, aerosol, and water vapor properties from the Moderate Resolution Imaging Spectrometer (MODIS)," *IEEE Trans. Geosci. Remote Sens.*, vol. 30, pp. 2-27, 1992.

[24] M. D. King, Y. J. Kaufman, D. Tanré, and T. Nakajima, "Remote sensing of tropospheric aerosols from space: Past, present, and future," *Bull. Amer. Meteor. Soc.*, vol. 80, pp. 2229-2259, 1999.

[25] M. D. King, W. P. Menzel, Y. J. Kaufman, D. Tanré, B. C. Gao, S. Platnick, S. A. Ackerman, L. A. Remer, R. Pincus, and P. A. Hubanks, "Cloud and aerosol properties, precipitable water, and profiles of temperature and humidity from MODIS," *IEEE Trans. Geosci. Remote Sens.*, vol. 41, pp. 442-458, 2003.

[26] K. Laval, "General circulation model experiments with surface albedo changes," *Climate Change*, vol. 9, pp. 91-102, 1986.

[27] Z. Q. Li and L. Garand, "Estimation of surface albedo from space – A parameterization for global application", *J. Geophys. Res.*, vol. 99 (D4), pp. 8335-8350, 1994.

[28] S. Liang. H. Fang, M. Chen, C. J. Shuey, C. Walthall, C. Daughtry, J. Morisette, C. Schaaf, and A. Strahler, "Validating MODIS land surface reflectance and albedo products: Methods and preliminary results," *Remote Sens. Environ.*, vol. 83, pp. 149-162, 2002.

[29] B. M. Lofgren, "Sensitivity of land-ocean circulations, precipitation, and soil moisture to perturbed land surface albedo," *J. Climate*, vol. 8, pp. 2521-2542, 1995.

[30] B. M. Lofgren, "Surface albedo climate feedback simulated using two-way coupling," *J. Climate*, vol. 8, pp. 2543-2562, 1995.

[31] C. L. Parkinson, "Aqua: An Earth-observing satellite mission to examine water and other climate variables," *IEEE Trans. Geosci. Remote Sens.*, vol. 41, pp. 173-183, 2003.

[32] J. Penuelas, I. Filella, X. Zhang, L. Llorens, R. Ogaya, F. Lloret, P. Comas, M. Estiarte, and J. Terradas, "Complex spatiotemporal phenological shifts as a response to rainfall changes," *New Phytologist*, vol. 161, pp. 837-846, 2004.

[33] R. T. Pinker and I Laszio, "Modeling surface solar irradiance for satellite applications on a global scale", *J. App. Meteo.*, vol. 31, pp. 194-211, 1992.

[34] S. Platnick, M. D. King, S. A. Ackerman, W. P. Menzel, B. A. Baum, J. C. Riédi, and R. A. Frey, "The MODIS cloud products: Algorithms and examples from Terra," *IEEE Trans. Geosci. Remote Sens.*, vol. 41, pp. 459-473, 2003.

[35] W. H. Press, S. A. Teukolsky, W. T. Vetterling, and B. P. Flannery, *Numerical Recipes in FORTRAN: The Art of Scientific Computing, 2nd Ed*, Cambridge University Press, Cambridge, pp. 650-700, 1992.

[36] B. C. Reed, J. F. Brown, D. VanderZee, T. R. Loveland, J. W. Merchant, and D. O. Ohlen, "Measuring phenological variability from satellite imagery," *J. Veg. Sci.*, vol. 5, pp. 703-714, 1994.

[37] A. Roesch, M. Wild, R. Pinker, and A. Ohmura, "Comparison of spectral surface albedos and their impact on the general circulation model simulated surface climate," *J. Geophys. Res.*, 107(D14), 4221, doi:10.1029/2001JD000809, 2002.

[38] C. B. Schaaf, F. Gao, A. H. Strahler, W. Lucht, X. W. Li , T. Tsang, N. C. Strugnell, X. Y. Zhang, Y. F. Jin, J. P. Muller, P. Lewis, M. Barnsley, P. Hobson, M. Disney, G. Roberts, M. Dunderdale, C. Doll, R. P. d'Entremont, B. X. Hu, S. L. Liang, J. L. Privette, and D. Roy, "First operational BRDF, albedo nadir reflectance products from MODIS," *Remote Sens. Environ.*, vol. 83, pp. 135-148, 2002.

[39] M. D. Schwartz, "Green-wave phenology," *Nature*, vol. 394, pp. 839-840, 1998.

[40] M. D. Schwartz and B. C. Reed, "Surface phenology and satellite sensor-derived onset of greenness: An initial comparison," *Int. J. Remote Sens.*, vol. 20, pp 3451-3457, 1999.

[41] P. J. Sellers, "Remote sensing of the land surface for studies of global change," in *NASA/GSFC International Satellite Land Surface Climatology Project Report*, Columbia, MD, 1993.

[42] P. J. Sellers, D. A. Randall, G. J. Collatz, J. A. Berry, C. B. Field, D. A. Dazlich, C. Zhang, and L. Bounoua, "A revised land surface parameterization (SiB2) for atmospheric GCMs. Part 1: Model formulation," *J. Climate*, vol. 9, pp. 676-705, 1996.

[43] P. J. Sellers, S. O. Los, C. J. Tucker, C. O. Justice, D. A. Dazlich, G. J. Collatz,

and D. A. Randall, "A revised land surface parameterization (SiB2) for atmospheric GCMs. Part II: The generation of global fields of terrestrial biophysical parameters from satellite data," *J. Climate*, vol. 9, pp. 706-737, 1996.

[44] S. Sitch, B. Smith, I. C. Prentice, A. Arneth, A. Bondeau, W. Cramer, J. O. Kaplan, S. Levis, W. Lucht, M. T. Sykes, K. Thonicke, and S. Venevsky, "Evaluation of ecosystem dynamics, plant geography and terrestrial carbon cycling in the LPJ dynamic vegetation model," *Global Change Biology*, vol. 9, pp. 161-185, 2003.

[45] Y. C. Sud and M. Fennessy, "A study on the influence of surface albedo on July circulation in semi-arid regions using the GLAS GCM," *J. Climatol*., vol. 2(2), pp. 105-125, 1982.

[46] P. Viterbo and A. K. Betts, "Impact on ECMWF forecasts of changes to the albedo of the boreal forests in the presence of snow," *J. Geophys. Res*., vol. 104, pp. 27803-27810, 1999.

[47] K. Wang, J. Liu, X. Zhou, M. Sparrow, M. Ma, Z. Sun, and W. Jiang, "Validation of the MODIS global albedo surface albedo product using ground measurements in a semidesert region on the Tibetan Plateau", *J. Geophys. Res.*, vol. 109 (D5), doi:10.1029/2003JD004229, 2004.

[48] M. A. White, P. E. Thornton, and S. W. Running. "A continental phenology model for monitoring vegetation responses to interannual climatic variability," *Global Biogeochem. Cycles*, vol. 11, pp. 217-234, 1997.

[49] C. H. Whitlock, T. P. Charlock, W. F. Staylor, R. T. Pinker, I. Laszlo, A. Ohmura, H. Gilgen, T. Konzelman, R. C. DiPasquale, C. D. Moats, S. R. LeCroy, and N. A. Ritchey, "First global WCRP shortwave surface radiation budget data set," *Bull. Amer. Meteor. Soc*., vol. 76, pp. 905-922, 1995.

[50] X. B. Zeng, M. Shaikh, Y. J. Dai, R. E. Dickinson, and R. Myneni, "Coupling

of the common land model to the NCAR community climate model," *J. Climate*, vol. 15, pp. 1832-1854, 2002.

[51] X. Zhang, M. A. Friedl, C. B. Schaaf, A. H. Strahler, J. C. F. Hodges, F. Gao, and B. C. Reed, "Monitoring vegetation phenology using MODIS," *Remote Sens. Environ.*, vol. 84, pp. 471-475, 2003.

TABLE CAPTIONS

Table I. White-sky Albedo Percent Decrease Between Full Growth and Full Decay Phenological States for Selected IGBP Ecosystem Classifications and Wavelengths at Latitudes Northward of 40°, from 2001 data.

Table II. Regions where Persistent Cloud Case Methodology is Applied. Each Statistical Latitude Belt Consists of Data from a 15° Belt Centered on the Processed Pixel's Latitude.

Table III. HDF File Sizes for the Spatially-Filled Albedo Product, Stored on One-Minute Spatial Resolution Climate Modeling Grids. As White-SKY and Black-Sky Data are Stored in Identical Formats, the Table Lists Only White-Sky Information.

Table IV. HDF File Sizes for Statistics Computed from the Spatially-Filled Albedo Product. A Single HDF File Contains Statistics, by Grid Cell or by Ecosystem Class in a Grid Cell, at a Defined Resolution for All Wavelengths over a Single 16-Day Period. As White-Sky and Black-Sky Data are Stored in Identical Formats, the Table Lists only White-Sky Information. There are 23 16-Day Periods per Year.

TABLE I

WHITE-SKY ALBEDO PERCENT DECREASE BETWEEN FULL GROWTH AND FULL DECAY PHENOLOGICAL STATES FOR SELECTED IGBP ECOSYSTEM CLASSIFICATIONS AND WAVELENGTHS AT LATITUDES NORTHWARD OF 40°, FROM 2001 DATA.

	Western Hemisphere				Eastern Hemisphere			
Ecosystem	0.55 μm	0.86 μm	1.63 μm	0.7-5.0	0.55 μm	0.86 μm	1.63 μm	0.7-5.0
Evergreen Needle Forest	27%	36%	37%	41%	38%	46%	37%	45%
Deciduous Needle Forest	23%	50%	28%	46%	30%	51%	34%	44%
Deciduous Broadleaf Forest	27%	57%	15%	47%	33%	56%	23%	49%
Mixed Forest	28%	49%	30%	46%	34%	54%	32%	47%
Closed Shrubs	27%	34%	26%	41%	31%	44%	27%	40%
Open Shrubs	23%	37%	23%	40%	28%	41%	25%	37%
Woody Savanna	22%	42%	19%	40%	29%	47%	26%	42%
Savanna	22%	43%	18%	38%	27%	46%	22%	42%
Grassland	21%	40%	19%	35%	25%	39%	22%	35%
Wetland	22%	46%	19%	43%	31%	40%	33%	43%
Cropland	20%	52%	15%	40%	29%	52%	24%	44%
Barren	36%	39%	31%	42%	30%	33%	29%	34%

Table II

REGIONS WHERE PERSISTENT CLOUD CASE METHODOLOGY IS APPLIED. EACH STATISTICAL LATITUDE BELT CONSISTS OF DATA FROM A 15° BELT CENTERED ON THE PROCESSED PIXEL'S LATITUDE.

Region	Latitude	Longitude
South America	20°N – 30°S	86°W – 35°W
Central Africa	20°N – 30°S	17.5°W – 48.25°E
India	36°N – 2°N	60.75°E – 91.25°E
Southeast Asia	38.75°N – 18.5°N	91.25°E – 123.5°E
Oceania	18.5°N – 19°S	91.25°E – 164°E

Table III

HDF FILE SIZES FOR THE SPATIALLY-FILLED ALBEDO PRODUCT, STORED ON ONE-MINUTE SPATIAL RESOLUTION CLIMATE MODELING GRIDS. AS WHITE-SKY AND BLACK-SKY DATA ARE STORED IN IDENTICAL FORMATS, THE TABLE LISTS ONLY WHITE-SKY INFORMATION.

Dataset	File Characteristic
Spatially-Complete Albedo Dataset	
Files per 16-day period (1 per wavelength)	10
16-day periods per year	23
Total annual number of files	230
Annual number of files per wavelength	23
Data volume per file	445 MB
Total 16-day data volume (all 10 wavelengths)	4.35 GB
Total annual data volume	100 GB
Total annual data volume for one wavelength	10 GB
MOD43B3 General QA Dataset (applied to all wavelengths)	
Files per 16-day period	1
Total annual number of files	23
Data volume per file	446 MB
Total annual data volume	10 GB
MOD43B3 Band-Specific QA Dataset (not applied to broadband data)	
Files per 16-day period (1 per wavelength)	7
Total annual number of files	161
Annual number of files per wavelength	23
Data volume per file	223 MB
Total 16-day data volume (7 specific wavelengths)	1.5 GB
Total annual data volume	35 GB
Total annual data volume for one wavelength	5 GB
Spatially-Complete QA Dataset	
Files per 16-day period (1 per wavelength)	10
Total annual number of files	230
Annual number of files per wavelength	23
Data volume per file:	446 MB
Total 16-day data volume (7 specific wavelengths):	4.35 GB
Total annual data volume:	100 GB
Total annual data volume for one wavelength:	10 GB

Table IV.

HDF FILE SIZES FOR STATISTICS COMPUTED FROM THE SPATIALLY-FILLED ALBEDO PRODUCT. A SINGLE HDF FILE CONTAINS STATISTICS, BY GRID CELL OR BY ECOSYSTEM CLASS IN A GRID CELL, AT A DEFINED RESOLUTION FOR ALL WAVELENGTHS OVER A SINGLE 16-DAY PERIOD. AS WHITE-SKY AND BLACK-SKY DATA ARE STORED IN IDENTICAL FORMATS, THE TABLE LISTS ONLY WHITE-SKY INFORMATION. THERE ARE 23 16-DAY PERIODS PER YEAR.

	By Grid Cell		By Ecosystem Class in Grid	
Grid Size	16-day File Size	Yearly Data Volume	16-day File Size	Yearly Data Volume
0.5° x 0.5°	40 MB	920 MB	712 MB	16 GB
1° x 1°	9.9 MB	227.7 MB	178 MB	4 GB
2° x 2°	2.5 MB	57.5 MB	45 MB	1 GB
3° x 3°	1.1 MB	25.3 MB	20 MB	460 MB
4° x 4°	653 KB	14.6 MB	11 MB	253 MB
5° x 5°	425 KB	9.5 MB	7.1 MB	163.3 MB
10° x 10°	120 KB	2.7 MB	1.8 MB	41.4 MB

Eric G. Moody received the B.S. and M.S. degrees in chemical engineering from the Pennsylvania State University in 1996 and 1998, and joined Goddard Space Flight Center through contract with SM&A Corporation (now L-3 Communications Government Services, Inc.).

He has more than 5 years' experience in satellite and aircraft data analysis and evaluation through work with the MODIS Science Team on the development of the cloud optical and microphysical property and Level-3 algorithms, user community software tools, visualization algorithms, and the implementation of ancillary datasets. He also has more then four years experience researching and modeling turbulent fluid dynamics, reaction chemistry, reactor design, and the evolution of particle size distributions through aerosol nucleation and coagulation.

Michael D. King (M'01–SM'03) received the B.A. degree in physics from Colorado College in 1971, and the M.S. and Ph.D. degrees in atmospheric sciences from the University of Arizona in 1973 and 1977, respectively.

He joined NASA Goddard Space Flight Center in January 1978 and is currently Senior Project Scientist of NASA's Earth Observing System (EOS), a position he has held since 1992. He is a member of the MODIS Science Team where he has primary responsibility for developing the cloud optical and microphysical property and Level-3 algorithms. His research experience includes conceiving, developing, and operating multispectral scanning radiometers from a number of aircraft platforms in field experiments ranging from arctic stratus clouds to smoke from the Kuwait oil fires in the Persian Gulf and biomass burning in Brazil and southern Africa.

Dr. King is a Fellow of the American Meteorological Society (AMS), recipient

of the AMS Verner E. Suomi Award for significant and fundamental contributions to remote sensing and radiative transfer, and recipient of the 1992 Transactions Prize Paper Award by the IEEE Geoscience and Remote Sensing Society. He is a member of the US National Academy of Engineering.

Steven Platnick received the B.S. degree in electrical engineering from Duke University in 1979, the M.S. degree in electrical engineering from the University of California Berkeley in 1980, and the Ph.D. degree in atmospheric sciences from the University of Arizona in 1991.

He joined NASA Goddard Space Flight Center in January 2003 and is currently Deputy Project Scientist of NASA's *Aqua* satellite. Prior to this appointment, he was a Research Associate Professor in the Joint Center for Earth Systems Technology, University of Maryland Baltimore County, a position he held from 1996-2002. He has worked in collaboration with NASA Goddard Space Flight Center since 1993, and prior to that held engineering positions at Hewlett-Packard Co. for 6 years as well as a National Research Council Resident Research Associate position at NASA Ames Research Center. His research experience includes theoretical and experimental studies of satellite, aircraft, and ground-based cloud remote sensing, including applications to MODIS. He is a member of the MODIS Science Team.

Crystal B. Schaaf (M'92) received the S.B. and S.M. degrees in meteorology from the Massachusetts Institute of Technology, Cambridge, in 1982, the M.L.A. degree in archaeology from Harvard University, Cambridge, MA, in 1988, and the Ph.D. degree in geography from Boston University, Boston, MA, in 1994.

She is a Research Associate Professor of Geography and Researcher in the Center for Remote Sensing, Boston University, and is a member of the MODIS

and NPP Science Teams. Her research interests cover remote sensing of land surfaces and clouds, with particular emphasis on surface anisotropy and albedo.

Feng Gao (M'99) received the B.A. degree in geology and the M.S. degree in remote sensing from Zhejiang University, Hangzhou, China, in 1989 and 1992, respectively, the Ph.D. degree in geography from Beijing Normal University, Beijing, China, in 1997, and the M.S. degree in computer science from Boston University, Boston, MA, in 2003.

From 1992 to 1998, he was a Research Scientist with the Nanjing Institute of Geography and Limnology, Chinese Academy of Science, Nanjing, China. Currently, he is a Research Associate Professor with the Department of Geography and Researcher in the Center for Remote Sensing, Boston University. He is working on NASA's MODIS BRDF/Albedo project. His research interests include remote sensing modeling and retrieving vegetation parameters through inversion of BRDF models using directional measurements.

FIGURE LEGENDS

Fig. 1. Phenological behavioral curves for deciduous broadleaf forest in Vermont, US, from July through December 2001, computed from (a) pixel-level data and statistical regions and (b) the same data with offsets applied to adjust the magnitudes to match pixel level detail.

Fig. 2. Global MOD43B3 white-sky albedo at 0.86 μm, based on remapping onto a one-minute resolution grid and with seasonal snow and pixels of lesser quality removed through application of quality assurance information, for 16-day periods of (a) January 1-16, (b) April 3-18, (c) July 12-27, and (d) September 30-October 14, 2001.

Fig. 3. Phenological behavioral curves for cropland in the Upper Midwestern US from July through December 2001, computed from (a) pixel-level data and statistical regions and (b) the same data with offsets applied to adjust the magnitudes to match pixel level detail.

Fig. 4. Comparison of white-sky albedo at 0.86 μm for the continental United States for the July 12-27, 2001 sixteen-day time period, where (a) is the conditioned MOD43B3 data, (b) the spatially complete data, and (c) the IGBP ecosystem classification map used during processing.

Fig. 5. Phenological behavioral curves for mixed forest in northern Russia for July through December 2001, computed from pixel-level data and statistical regions with offsets applied to adjust the magnitudes to match pixel-level detail. For this case, the full decay state is not observed for even the 10° x 10° region; therefore the general methodology is modified by computing the full decay state based on the full growth value.

Fig. 6. Comparison of white-sky albedo at 0.86 μm for Europe and western Asia for the December 3-18, 2001 sixteen-day time period, where (a) is the

conditioned MOD43B3 data, (b) the spatially complete data, and (c) the IGBP ecosystem classification map used during processing.

Fig. 7. Comparison of white-sky albedo at 0.86 μm for the Indian subcontinent for the May 25–June 9, 2001 sixteen-day time period, where (a) is the conditioned MOD43B3 data, (b) the spatially complete data, and (c) the IGBP ecosystem classification map used during processing.

Fig. 8. Comparison of white-sky albedo at 0.86 μm for central and southern Africa, for the December 3-18, 2001 sixteen-day time period, where (a) is the conditioned MOD43B3 data, (b) the spatially complete data, and (c) the IGBP ecosystem classification map used during processing.

Fig. 9. Spatially complete white-sky albedo at 0.86 μm after the temporal interpolation technique was applied for the 16-day periods of (a) January 1-16, (b) April 3-18, (c) July 12-27, and (d) September 30-October 14, 2001.

Fig. 10. Spatially complete white-sky albedo as a function of wavelength for a region encompassing London, England, and Paris, France, for a selection of IGBP ecosystem classifications and for the 16-day period from June 26-July 11, 2001.

Fig. 11. White-sky albedo as a function of wavelength for a region encompassing London, England, and Paris, France, for (a) cropland and (b) urban ecosystem, computed from the spatially complete dataset for 16-day periods from January through July 2001.

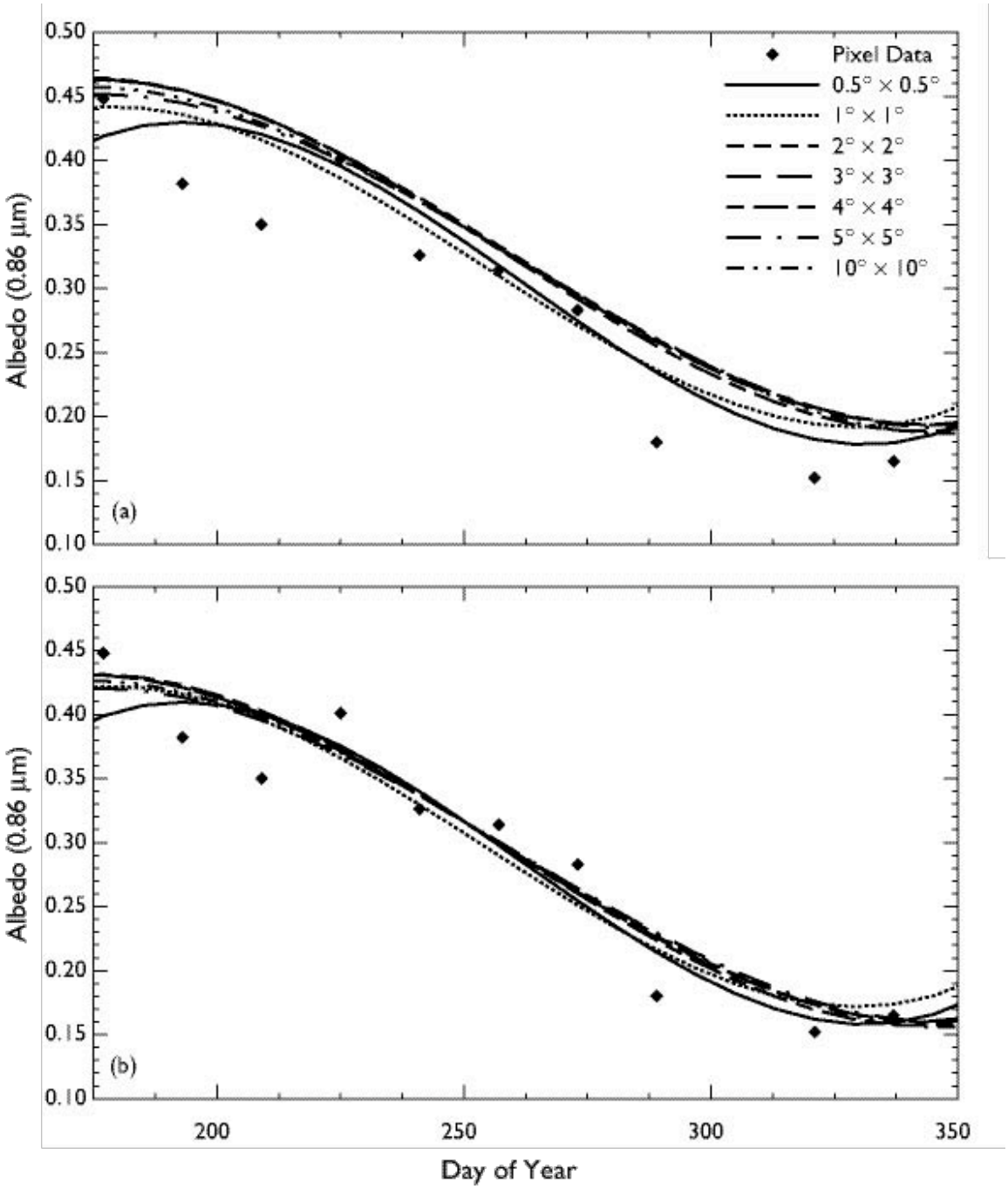

Fig. 1. Phenological behavioral curves for deciduous broadleaf forest in Vermont, US, from July through December 2001, computed from (a) pixel-level data and statistical regions and (b) the same data with offsets applied to adjust the magnitudes to match pixel level detail.

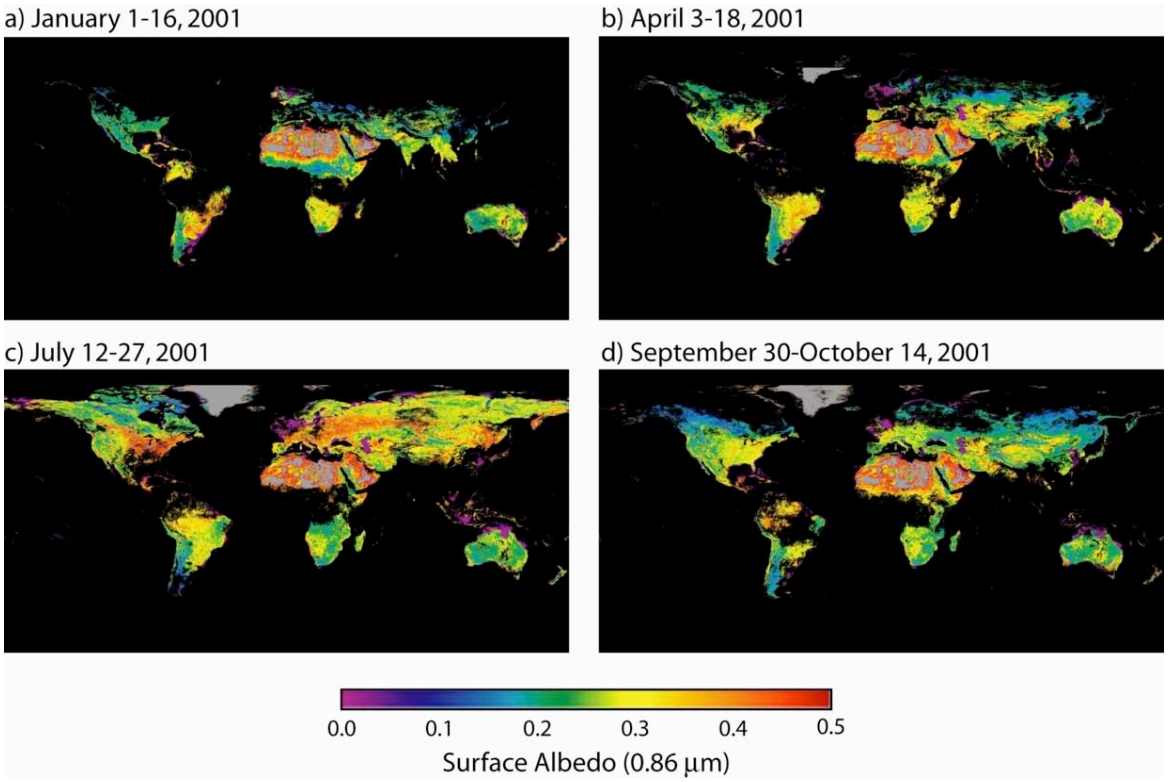

Fig. 2. Global MOD43B3 white-sky albedo at 0.86 μm, based on remapping onto a one-minute resolution grid and with seasonal snow and pixels of lesser quality removed through application of quality assurance information, for 16-day periods of (a) January 1-16, (b) April 3-18, (c) July 12-27, and (d) September 30-October 14, 2001.

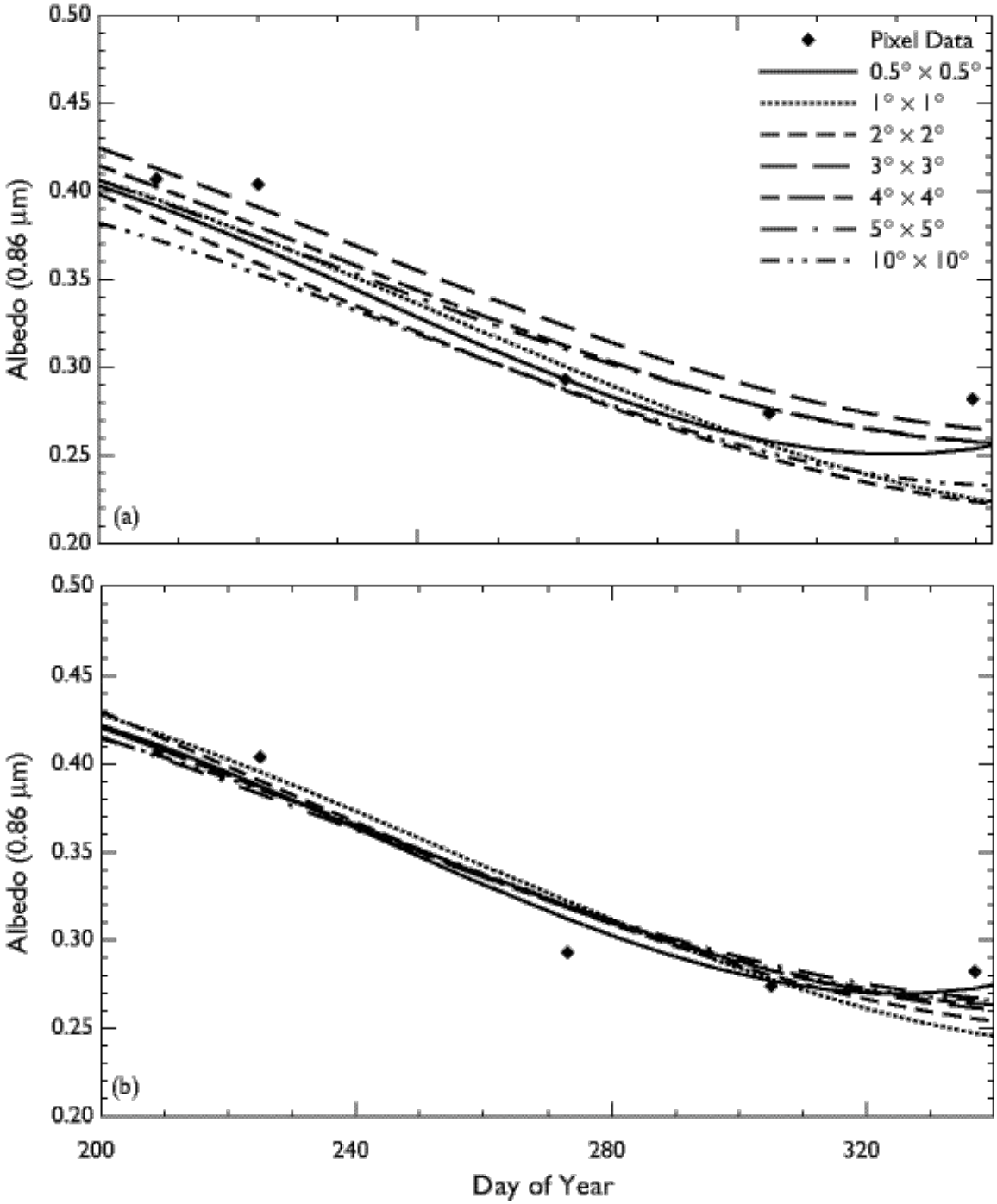

Fig. 3. Phenological behavioral curves for cropland in the Upper Midwestern US from July through December 2001, computed from (a) pixel-level data and statistical regions and (b) the same data with offsets applied to adjust the magnitudes to match pixel level detail.

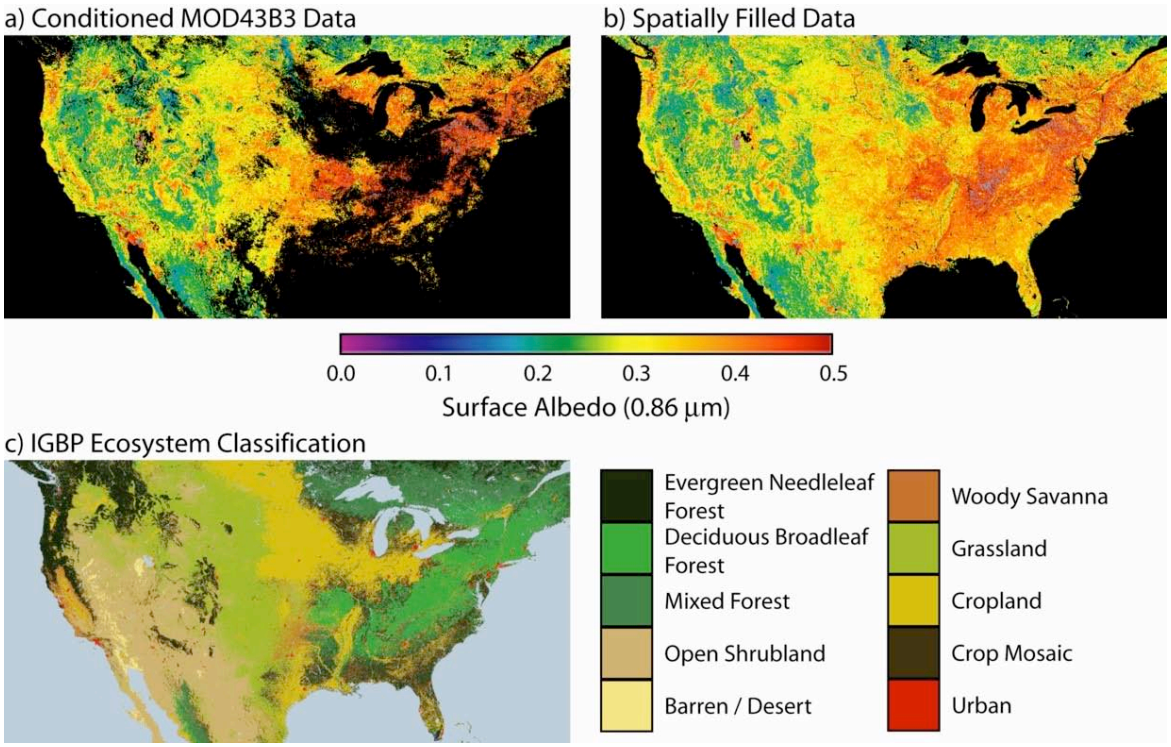

Fig. 4. Comparison of white-sky albedo at 0.86 μm for the continental United States for the July 12-27, 2001 sixteen-day time period, where (a) is the conditioned MOD43B3 data, (b) the spatially complete data, and (c) the IGBP ecosystem classification map used during processing.

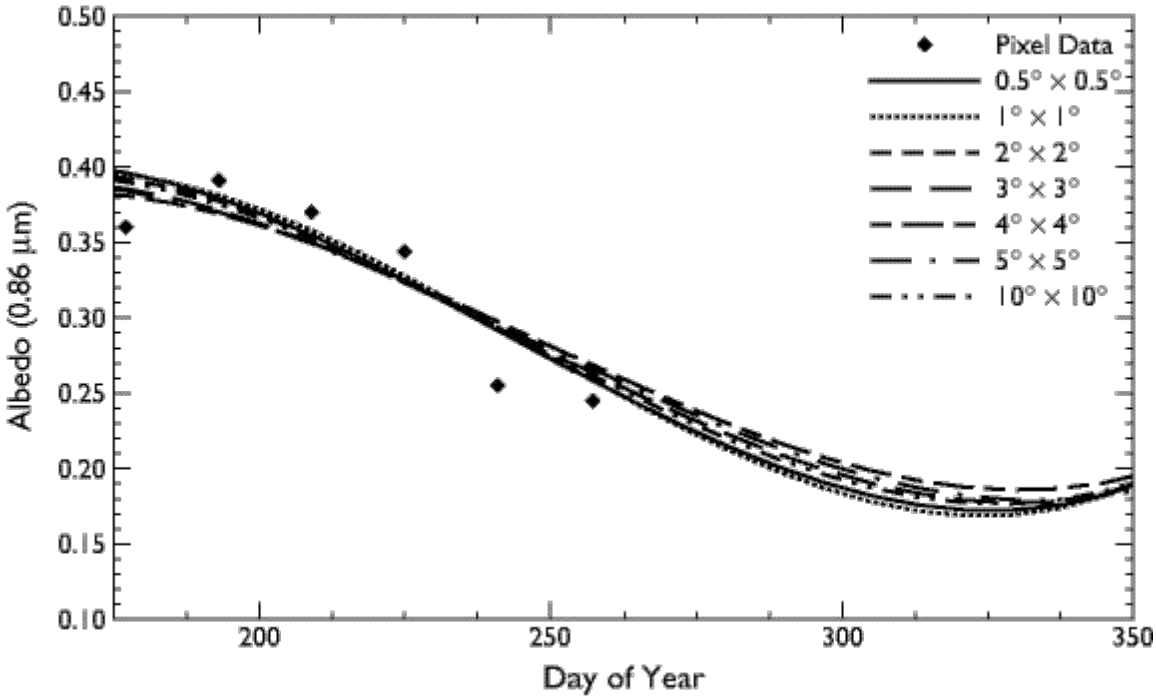

Fig. 5. Phenological behavioral curves for mixed forest in northern Russia for July through December 2001, computed from pixel-level data and statistical regions with offsets applied to adjust the magnitudes to match pixel-level detail. For this case, the full decay state is not observed for even the 10° x 10° region; therefore the general methodology is modified by computing the full decay state based on the full growth value.

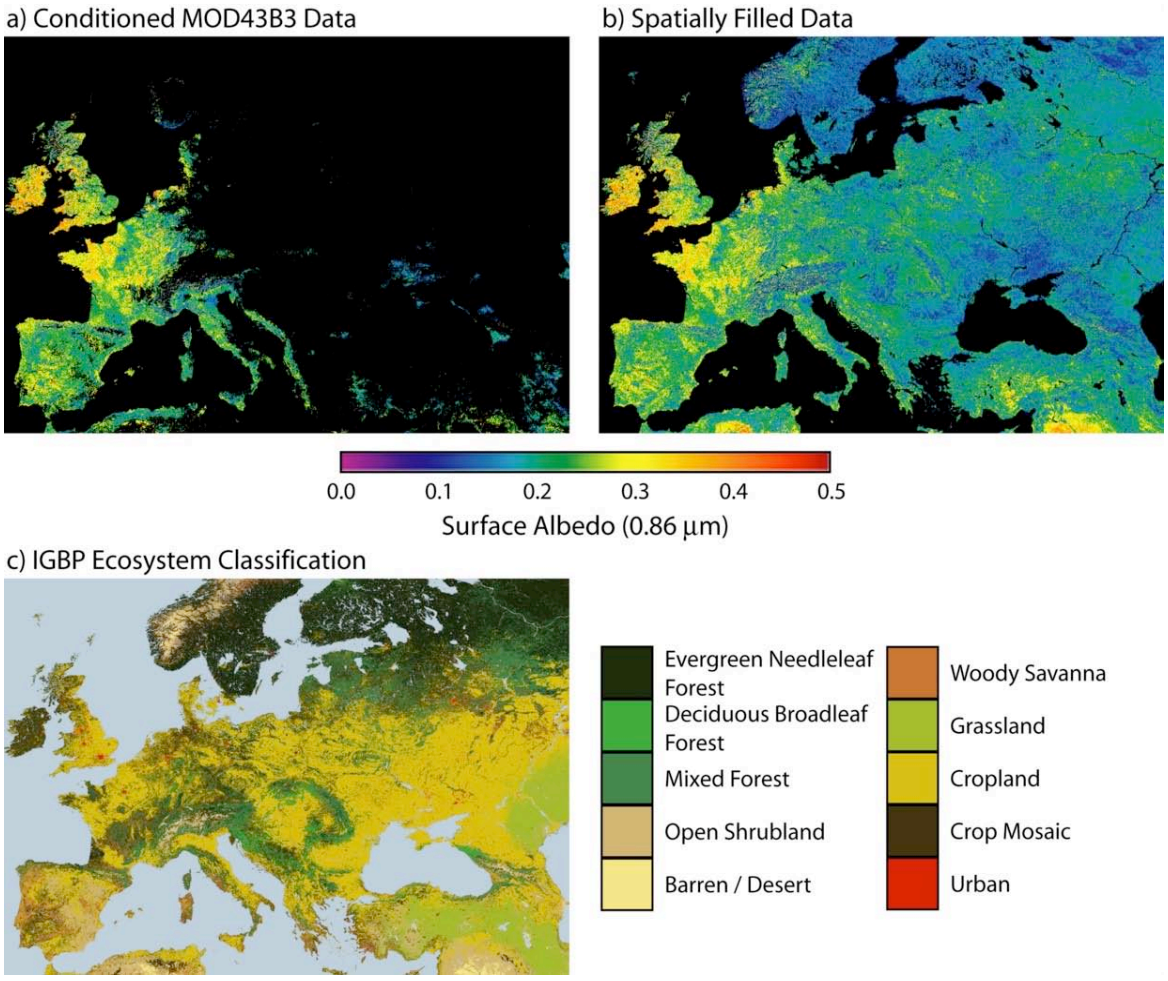

Fig. 6. Comparison of white-sky albedo at 0.86 μm for Europe and western Asia for the December 3-18, 2001 sixteen-day time period, where (a) is the conditioned MOD43B3 data, (b) the spatially complete data, and (c) the IGBP ecosystem classification map used during processing.

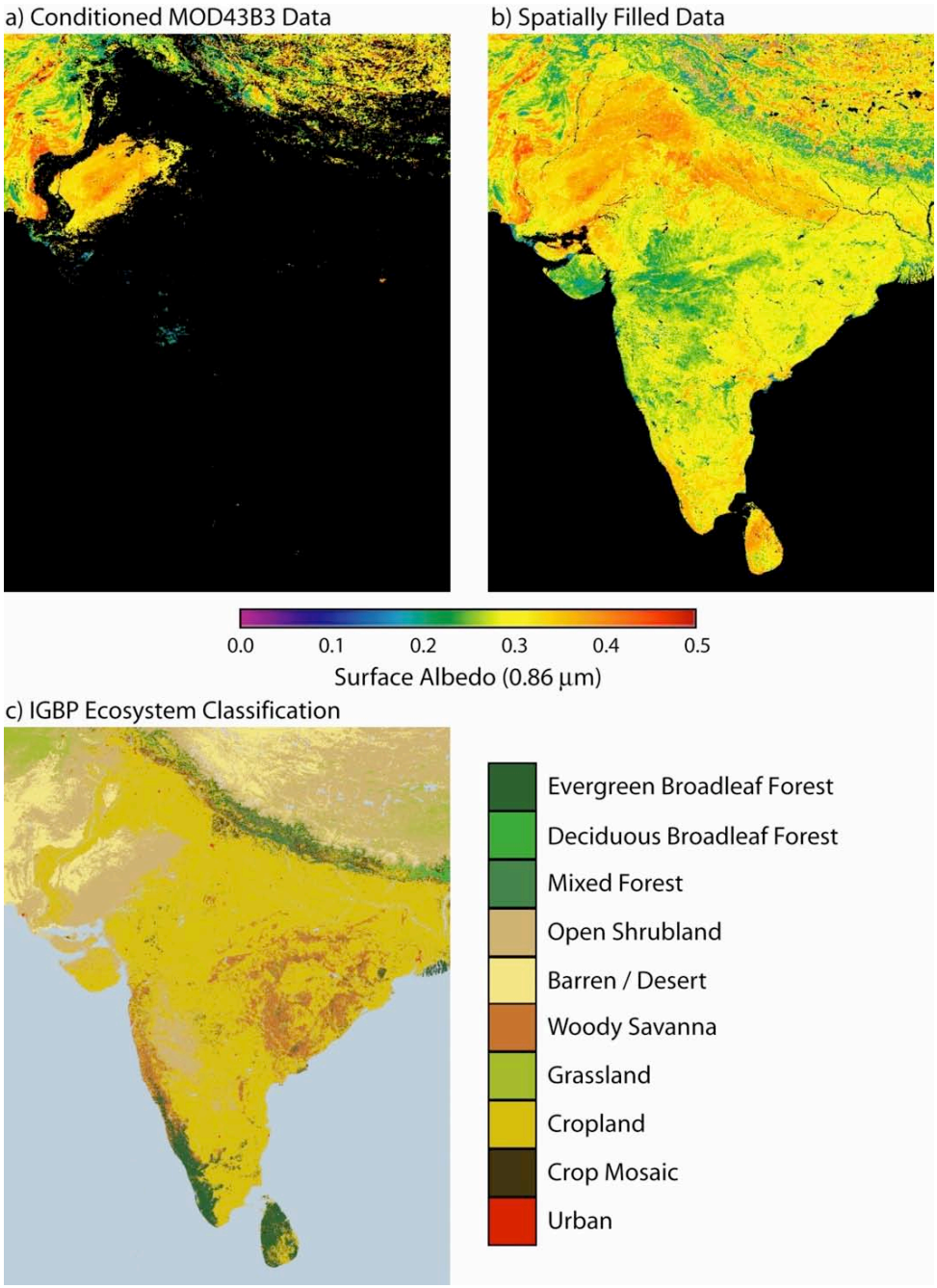

Fig. 7. Comparison of white-sky albedo at 0.86 μm for the Indian subcontinent for the May 25–June 9, 2001 sixteen-day time period, where (a) is the conditioned MOD43B3 data, (b) the spatially complete data, and (c) the IGBP ecosystem classification map used during processing.

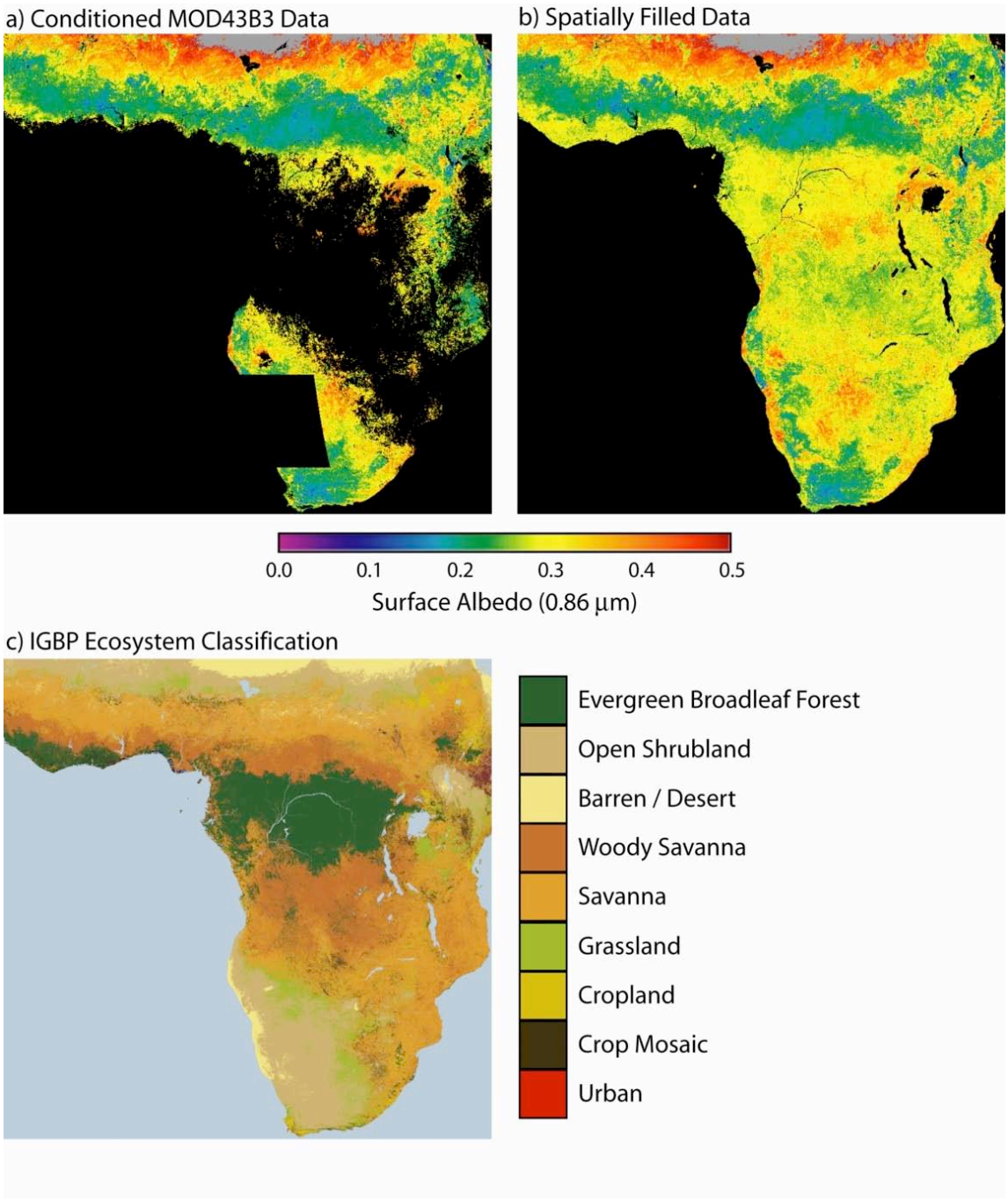

Fig. 8. Comparison of white-sky albedo at 0.86 μm for central and southern Africa, for the December 3-18, 2001 sixteen-day time period, where (a) is the conditioned MOD43B3 data, (b) the spatially complete data, and (c) the IGBP ecosystem classification map used during processing.

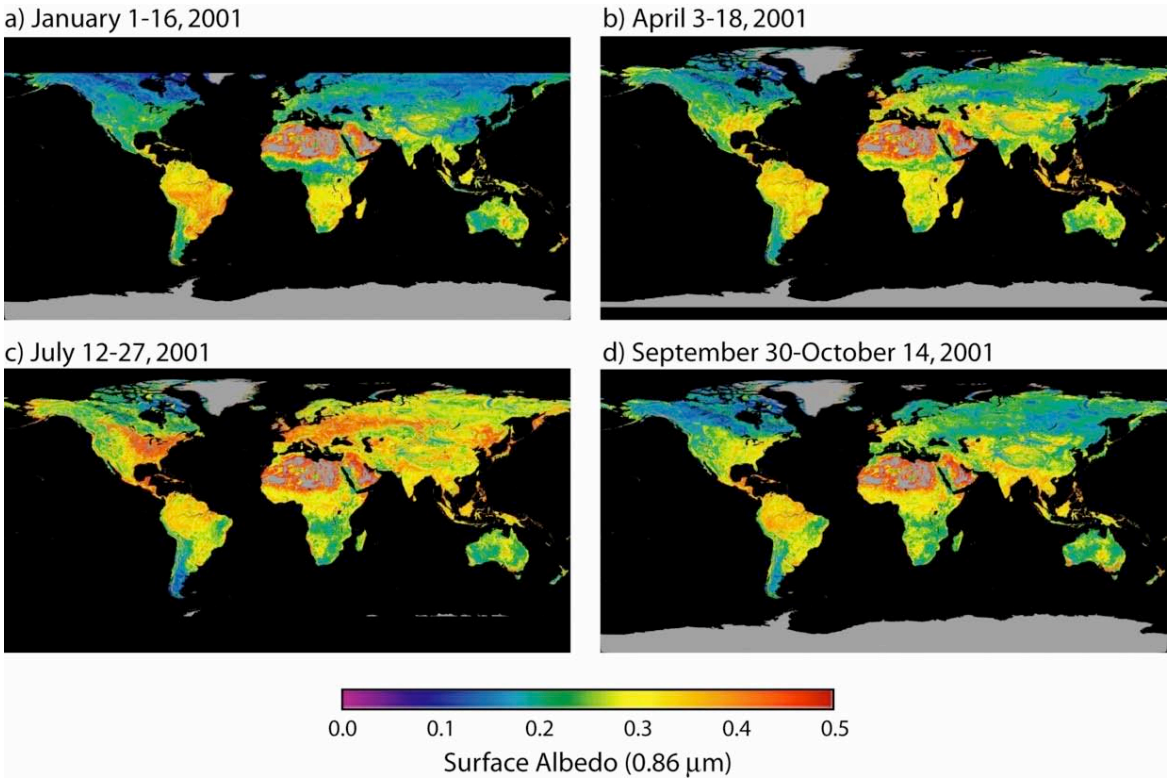

Fig. 9. Spatially complete white-sky albedo at 0.86 μm after the temporal interpolation technique was applied for the 16-day periods of (a) January 1-16, (b) April 3-18, (c) July 12-27, and (d) September 30-October 14, 2001.

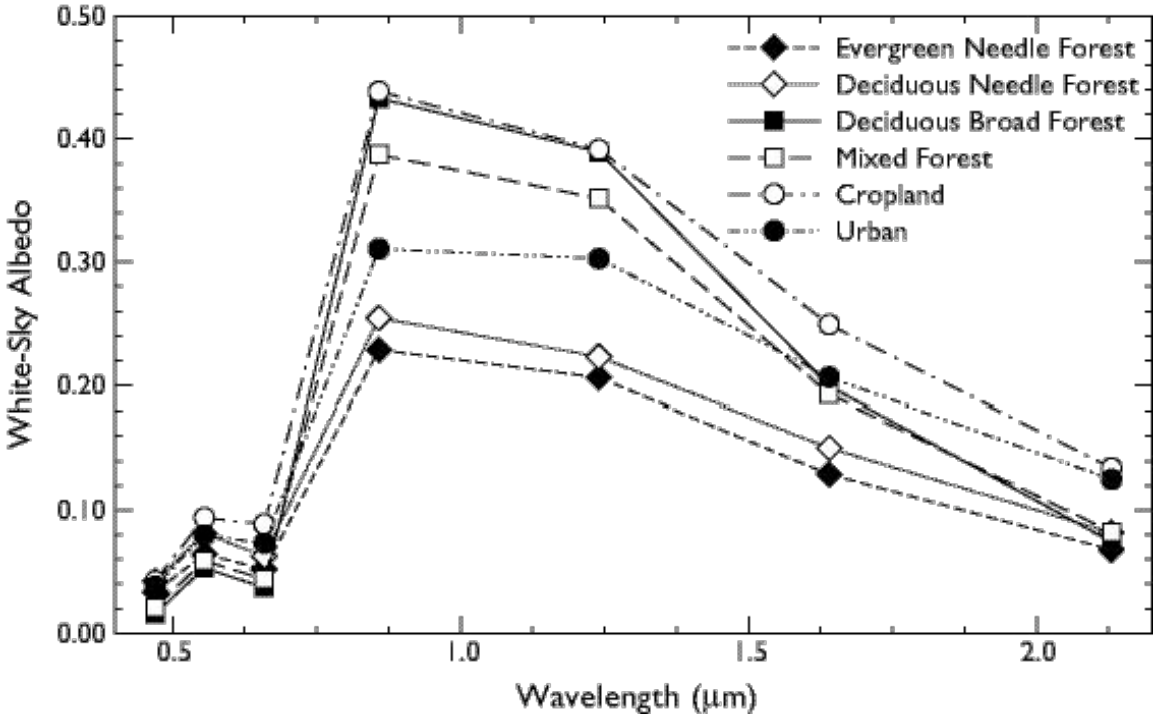

Fig. 10. Spatially complete white-sky albedo as a function of wavelength for a region encompassing London, England, and Paris, France, for a selection of IGBP ecosystem classifications and for the 16-day period from June 26-July 11, 2001.

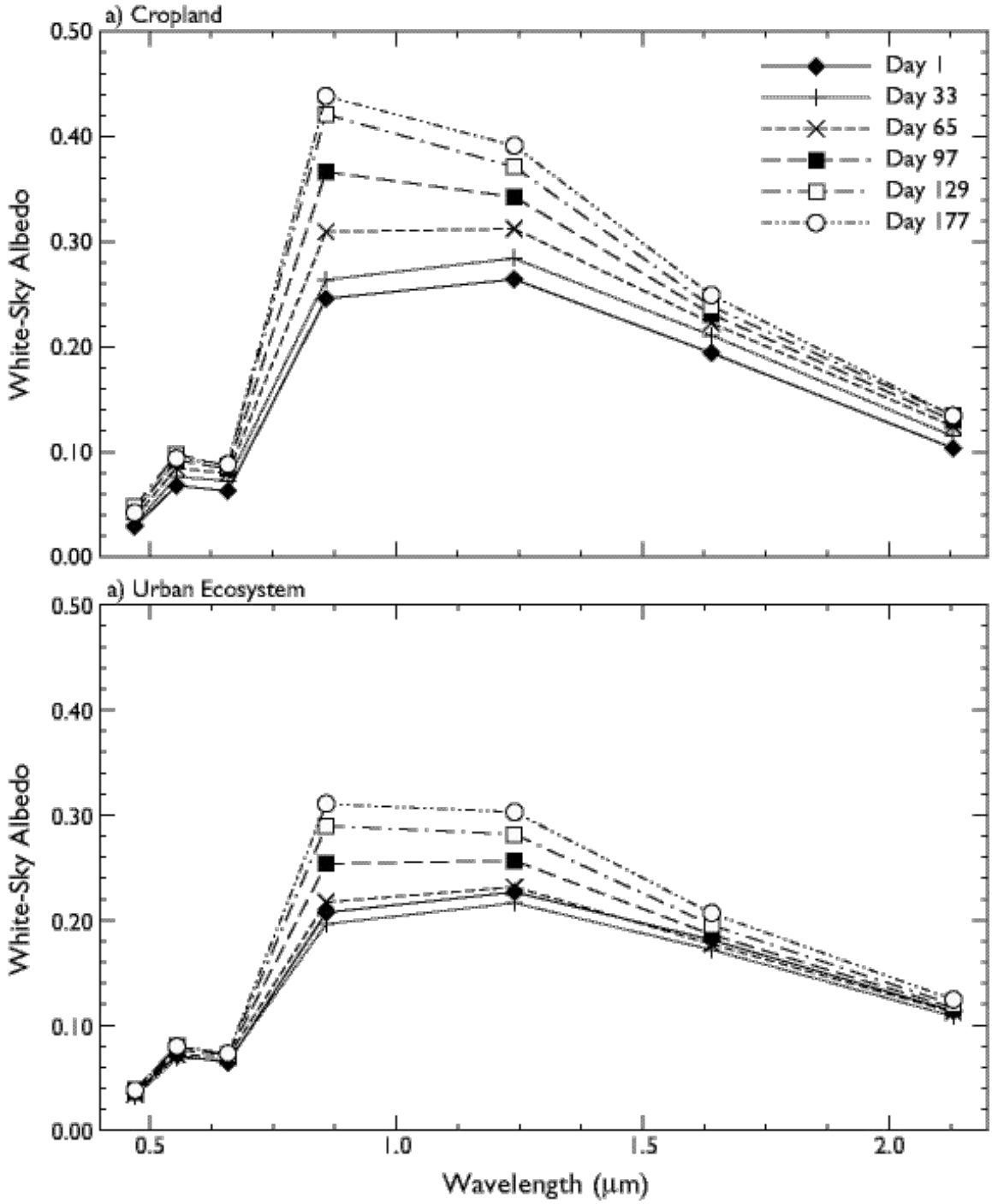

Fig. 11. White-sky albedo as a function of wavelength for a region encompassing London, England, and Paris, France, for (a) cropland and (b) urban ecosystem, computed from the spatially complete dataset for 16-day periods from January through July 2001.